Optics Letters

Temperature-compensated optical fiber sensor for volatile organic compound gas detection based on cholesteric liquid crystal

Jianyang Hu,[1] Yuzhou Chen,[1] Zhenyu Ma,[1] Li Zeng,[1] Dong Zhou,[1] Zenghui Peng,[2] Weimin Sun,[1] and Yongjun Liu[1,2,*]

[1]Key Lab of In-fiber Integrated Optics, Ministry Education of China, Harbin Engineering University, Harbin 150001, China
[2]State Key Laboratory of Applied Optics, Changchun Institute of Optics, Fine Mechanics and Physics, Chinese Academy of Sciences, Changchun 130033, China
*Corresponding author: liuyj@hrbeu.edu.cn

Received 13 April 2021; revised 11 June 2021; accepted 13 June 2021; posted 14 June 2021 (Doc. ID 427606); published 6 July 2021

External temperature variations inevitably affect the accuracy of a liquid crystal sensor. Therefore, we propose a novel temperature-compensated fiber volatile organic compound (VOC, using acetone as a model compound) gas sensor. The proposed sensor consists of a short segment of hollow-core fiber (HCF), which is spliced on a multimode fiber. Cholesteric liquid crystal (CLC) is sealed into HCF to sense the temperature, and another type of CLC is coated on the end face of HCF for VOC gas detection. The VOC gas concentration and ambient temperature can be simultaneously measured by monitoring the wavelength shifts of two Bragg reflection peaks caused by two types of CLCs. The effects of the CLC thickness on the sensitivities of temperature and acetone concentration are investigated, and optimal parameters are chosen. An optimal sensor can reach a temperature sensitivity of 2.53 nm/°C and acetone concentration sensitivity of 48.46 nm·L/mmol at 8–44°C. In addition, temperature compensation capability, repeatability, response time, and stability are also researched. The experimental results prove this sensor has great application potential in high-precision real-time VOC gas monitoring and detection.

https://doi.org/10.1364/OL.427606

As one of the most common gaseous pollutants, a volatile organic compound (VOC) can cause many harmful effects on human health. Therefore, it is important to detect and monitor VOC gases in outdoor and indoor air [1]. The most popular detection methods rely on resistive-based VOC gas sensors [2], gas chromatography/mass spectrometry [3], or ion mobility spectrometry [4]. Although these methods have excellent sensitivity or precision in detecting VOC gases, the bulky and expensive equipment and complicated experimental preparation make them unsuitable for real-time VOC gas detection. The fiber sensor provides an alternative option for VOC gas detection with the advantages of being ultra-compact and having low cost and rapid response [5].

The remarkable molecular reconfiguration ability makes the liquid crystal (LC) extremely sensitive to external stimuli such as temperature [6], electric field [7], pH value [8], and volatile gas [9]. Among various optically anisotropic LC materials, cholesteric LC (CLC) has attracted special attention due to its supramolecular self-assembled helical structure and selective reflection characteristics. The structure of CLC is established by the continuous rotation and self-organization of rod-shaped LC molecules under the action of chiral molecules [10]. The distance between the LC molecular layers in which LC molecules rotate 2π is known as the pitch. According to changes in the external environment, CLC molecules can simply and quickly be reoriented. Therefore, even slight changes in the molecular scale can be easily detected by the twisted helical structure of CLC molecules [11].

Studies have shown that when CLC molecules are exposed to VOC gases, the pitch will change due to the interaction between CLC molecules and diffused VOC gas molecules. As a result, the Bragg reflection band will vary accordingly. Several VOC gas sensors based on LC mixtures [12], polymer-stabilized CLC [13], and CLC film [14] have been reported. However, these sensors can only qualitatively detect the VOC gas concentration from the color change of the reflected light caused by the Bragg reflection of CLC, but cannot accurately detect the VOC gas concentration. Chang *et al*. realized the quantitative detection of acetone and toluene vapors concentration by analyzing the spectrum of reflected light from CLC [15]. Tang *et al*. coated a layer of CLC on the side-polished fiber surface to achieve an optical fiber-based VOC gas sensor [16], in which the measured sensitivity of the acetone vapor reached 3.46 nm·L/mmol. In our previous work, we proposed a CLC-based dual-probe VOC gas sensor to measure mixed VOC gases [17]. Nowadays, LC-based fiber VOC gas sensors have better performance than other sensors due to their compactness, low cost, and fast response. However, temperature cross talk is still the major problem to be solved.

In this Letter, we design and fabricate a novel temperature-compensated optical fiber VOC gas sensor. The fiber probe consists of a segment of a hollow-core fiber (HCF), which is filled with CLC and sealed with a UV curing adhesive for temperature monitoring. The end surface of HCF is coated

with another type of CLC for simultaneous VOC gas sensing. Acetone is an important organic solvent in industry, and acetone vapor in the environment poses a health risk to humans. In addition, the concentration detection of acetone vapor from exhaled breath of patients is an effective method for diagnosing diabetes [18], so we use it as a model compound for testing. Different CLCs reflect light with different wavelengths through Bragg reflection. Therefore, two separate Bragg reflection peaks are observed in the reflection spectrum of this optical fiber sensor. The peak with a longer wavelength is used to detect the VOC gas concentration, and the other peak serves as temperature compensation. When this proposed CLC-based fiber VOC gas sensor is exposed to acetone with different vapor concentrations, the characteristics of sensitivity, temperature compensation, response time, repeatability, and stability are researched. For the first time, to our knowledge, we propose and prove a method to solve the temperature cross talk problem of the LC-based VOC gas sensor.

CLCs used here are mixtures of cholesteryl chloroformate, cholesterol oleyl carbonate, and cholesteryl chloride from InnoChem, Beijing. Considering the range of the light source and the subsequent sensing requirements, two types of CLCs are prepared: CLC1 consists of 11.7 wt% cholesteryl chloride, 66.7 wt% cholesterol oleyl carbonate, and 21.6 wt% cholesteryl chloroformate. CLC2 contains 19.2 wt% cholesteryl chloride, 57.7 wt% cholesterol oleyl carbonate, and 23.1 wt% cholesteryl chloroformate. These two CLC mixtures are first heated to 120°C for 10 min and then ultrasonicated for 30 min to thoroughly mix the three cholesteryl derivatives. Finally, the mixtures are naturally cooled to room temperature.

A schematic diagram of a VOC gas sensing probe is shown in Fig. 1. An HCF with a length of 120 μm, inner diameter of 30 μm, and outer diameter of 150 μm is first spliced on a multimode fiber (MMF) with a core diameter of 62.5 μm using a fusion splicer (FSM-80S, from Fujikura). Then CLC1, polyglycerin-10 (Shandong Yousuo Chemical Technology Co., Ltd.), and UV glue (LEAFTOP 9310) are sequentially injected into HCF through a tapered microtube (about 15 μm in diameter). The tapered microtube is made by flame heating and tapering technology, and the microtube is connected to a needle tube and allows fluid to be freely drawn or injected. By controlling the amount of CLC extracted each time, the thickness of the filled liquid crystal can be precisely controlled. Since CLC is soluble in the UV glue, polyglycerin-10 is used to separate CLC from the UV glue. This sandwich structure ensures that CLC1 will not be affected by the external VOC gas. Finally, the end face of HCF is coated with CLC2 through a finer microtube for VOC gas sensing.

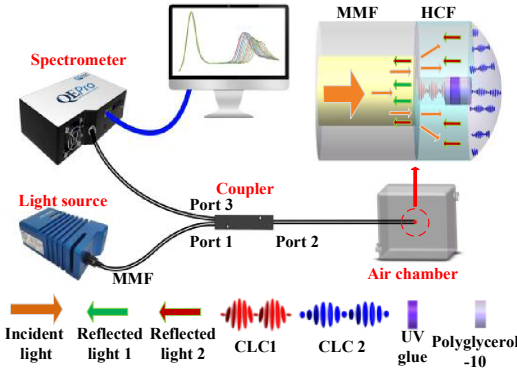

Fig. 1. Schematic of the experimental setup for the VOC gas sensor. The inset shows the schematic of a probe structure.

In the experimental system (Fig. 1), a tungsten halogen lamp (HL2000, Ideaoptics Inc., spectral range 360–2500 nm, input power 9 W) is employed as the light source and launches white light into a port (port 1) of a 1 × 2 MMF coupler. The VOC gas probe spliced with MMF (port 2) is fixed into a gas chamber. The reflected light from the sensor probe is collected through port 3 and sent to an optical spectrum analyzer with a spectral range of 300–1100 nm and resolution of 0.14 nm (QEpro, Ocean Optics Inc.). A computer is used to monitor, record, and analyze the reflection spectra. The temperature of the gas chamber is monitored by a commercial thermometer with a resolution of 0.1°C and can be changed by a heating platform. When a certain amount of VOC solvent is injected into this sealed gas chamber, the solvent quickly evaporates into gas. As a result, the VOC gas concentration changes accordingly.

The reflection spectra in different structures are exhibited in Fig. 2(a). The green line shows the original reflection spectrum from the empty HCF cavity, which corresponds to the microscope image in Fig. 2(b). The spectral bandwidth of the selective Bragg reflection is $\Delta\lambda = \Delta np$, where $\Delta n = n_e - n_o$ is the birefringence of the CLC, and p represents the helical pitch of CLC. The blue line displays the Bragg reflection spectrum from the CLC1-filled HCF cavity [Fig. 2(c)], and the wavelength of the Bragg reflection peak is 630 nm. The red line shows the Bragg reflection spectrum from the HCF cavity coated with CLC2 on the fiber end face [Fig. 2(d)], and the wavelength of the Bragg reflection peak is 770 nm. Compared with CLC2, CLC1 has a higher mixing ratio of cholesterol oleyl carbonate. Therefore, the wavelength of the CLC1 Bragg reflection peak is shorter. The reflection spectrum of the proposed sensor is displayed with the black line, and the wavelengths of the two Bragg reflection peaks are 630 and 770 nm. The microscope image and polarization micro-image of the sensor probe are shown in Figs. 2(e) and 2(f), respectively.

When the CLC1 thicknesses in HCF are 10, 20, 30, 40, 50, and 60 μm, the temperature sensitivities are 2.33, 2.28, 2.58, 2.31, 2.41, and 2.36 nm/°C, respectively. When the CLC2 coating thicknesses on the HCF end face are 10, 20, 30, 40, 50, and 60 μm, the acetone gas sensitivities are 47.41, 46.14, 46.83, 43.54, 42.92, and 43.35 nm·L/mmol, respectively. The sensor presents the highest temperature sensitivity at the CLC1 thickness of 30 μm, and the acetone gas sensitivity is slightly affected

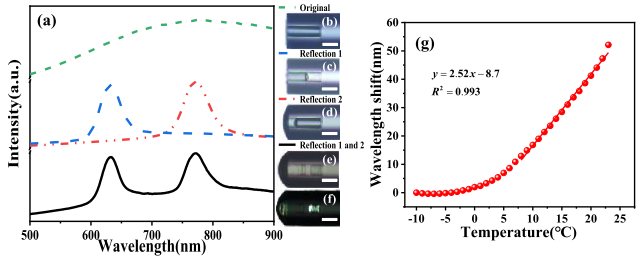

Fig. 2. (a) Reflection spectra from empty HCF (green line), CLC1-filled HCF (blue line), HCF with end coated CLC2 (red line), and proposed VOC gas sensor (black line). (b) Microscope image of HCF without CLC. (c) Microscope image of CLC1-filled HCF. (d) Microscope image of HCF coated with CLC2. (e) Microscope image of the sensor probe. (f) Polarization micro-image of the sensor probe. (g) Dependence of the reflection peak wavelength on temperature. The scale bar is 50 μm.

by the thickness of CLC2. Therefore, in the following experiments, the thicknesses of CLC1 and CLC2 are both chosen to be 30 μm to obtain better sensing results. Because LC materials become solid crystals in a cold environment, the temperature response of the sensor at low temperatures is measured. The sensor's response to temperature at low temperatures is nonlinear, as shown in Fig. 2(g). The sensor's response to temperature returns to linear after 8°C, so the temperature range of the sensor should be higher than 8°C. The clearing point of the CLC used in this letter is 44°C. Therefore, the working temperature range of the VOC gas sensor is 8–44°C.

The pitch of CLC increases with the rise of temperature. As a result, the wavelength of the Bragg reflection peak drifts with the fluctuation of the ambient temperature. By varying the internal temperature of the gas chamber, the temperature characteristics of the sensor can be tested. Figure 3(a) presents the reflection spectra of the VOC gas sensor at different temperatures. Both reflection peak wavelengths exhibit a redshift as the temperature rises from 25°C to 37°C. The wavelength of peak1 (generated by CLC1) moves from 635.55 to 667.86 nm, and the wavelength of peak2 (generated by CLC2) shifts from 778.64 to 839.67 nm. The dependence of the peak wavelength on the chamber temperature is shown in Fig. 3(b). A significant linear relationship between temperature and peak wavelength is exhibited. The sensitivities of peak1 and peak2 at the temperature range of 22°C to 38°C are 2.53 and 4.72 nm/°C with linear correlation coefficients of 0.994 and 0.989, respectively. This experimental result proves that our probe has excellent temperature sensing performance and can serve as temperature compensation for the subsequent VOC gas detection.

Figure 4(a) presents the reflective spectra of the VOC gas sensor exposed to different concentrations of acetone vapor. When the acetone concentration increases, the wavelength of peak2 significantly shifts to the red side because acetone gas molecules stimulate CLC2 molecules to expand the pitch, whereas the wavelength of peak1 remains unchanged because CLC1 sealed in HCF has no chance to interact with the external acetone vapor. The slight deviation of the peak1 wavelength is induced by small fluctuations in the ambient temperature. The wavelength of peak2 increases from 780.15 to 826.25 nm as the concentration of acetone gas rises from 0 to 0.946 mmol/L. The relationships between the acetone concentration and two peak wavelengths are exhibited in Fig. 4(b). The sensitivity of peak2 is 48.46 nm·L/mmol with a linear correlation coefficient of 0.996.

To investigate the temperature compensation capability of the VOC gas sensor, we select several environments that may cause temperature fluctuations. In Fig. 5, the black dot represents the peak1 wavelength shift $\Delta\lambda_{peak1}$ caused by temperature variation, the red dot indicates the peak2 wavelength

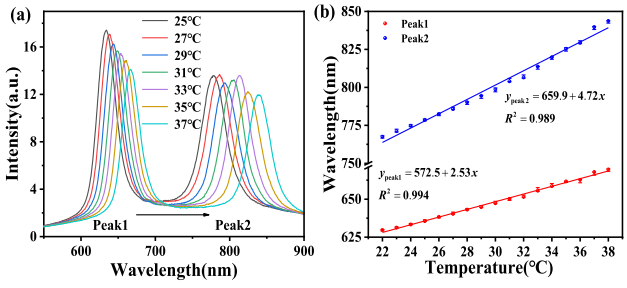

Fig. 3. (a) Reflection spectra of the VOC gas sensor at different temperatures. (b) Dependence of the peak wavelength on temperature.

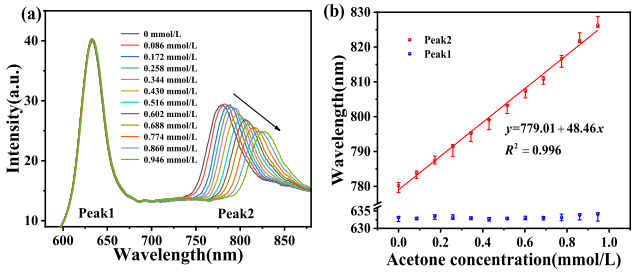

Fig. 4. (a) Reflection spectra at different acetone vapor concentrations. (b) Dependence of the peak wavelength on the concentration of acetone vapor.

shift $\Delta\lambda_{peak2}$ caused by acetone concentration and temperature changes, and the blue dot implies the actual peak2 wavelength shift $\Delta\lambda_{actual}$ caused only by the acetone concentration change, which can be calculated by the following equation:

$$\Delta\lambda_{actual} = \Delta\lambda_{peak2} - \frac{\Delta\lambda_{peak1} \cdot S_{peak2}}{S_{peak1}}, \quad (1)$$

where S_{peak1} and S_{peak2} are temperature sensitivities of peak1 and peak2, respectively, and $S_{peak1} = 2.53$ nm/°C and $S_{peak2} = 4.7$ nm/°C. Figure 5(a) presents the acetone gas concentration sensing under the temperature fluctuation induced by airflow. Airflow has a weak effect on temperature. Without temperature compensation, the peak2 gas sensitivity is 51.57 nm·L/mmol with a linear correlation coefficient of 0.989. After temperature compensation, the acetone vapor sensitivity is 46.45 nm·L/mmol with a linear correlation coefficient of 0.996. It is obvious that the sensing accuracy is improved after temperature compensation. Figures 5(b) and 5(c) show the sensing results under temperature fluctuations caused by far-distance and near-distance human breathing, respectively. After temperature compensation, the linear correlation coefficients increase from 0.986 to 0.994 for far-distance human breathing (about 30 cm), and from 0.983 to 0.988 for near-distance human breathing (about 10 cm). To test the limit of temperature compensation capability, we create a rapid temperature fluctuation environment. As shown in Fig. 5(d), the temperature seriously disturbs the gas concentration sensing of peak2, and the linear relationship between the wavelength shift of peak2 and acetone concentration is destroyed. Obviously, using a gas sensor with a linear correlation coefficient of only 0.569 is unreliable. However, after temperature compensation, the linear correlation coefficient improves to 0.977. The linear correlation coefficients after temperature compensation do not reach normal values due to deviations in the experimental process and data processing. Therefore, this gas sensor can efficiently compensate for the influence of temperature fluctuations in the VOC gas detection process.

The dynamical sensing characteristics of our sensor are researched by repeatedly switching the acetone concentration. In the experiment, 0.1 mmol acetone solvent is first injected into the 500 mL gas chamber by a syringe. Acetone quickly evaporates into the gas chamber, and the acetone concentration increases from 0 to 0.2 mmol/L. Meanwhile, the reflection spectra are recorded in real time. Then, after the reflection spectrum is stable, the sensor probe is rapidly removed from the gas chamber. Finally, after the reflection spectrum is stable again, the sensor probe is placed back into the gas chamber to

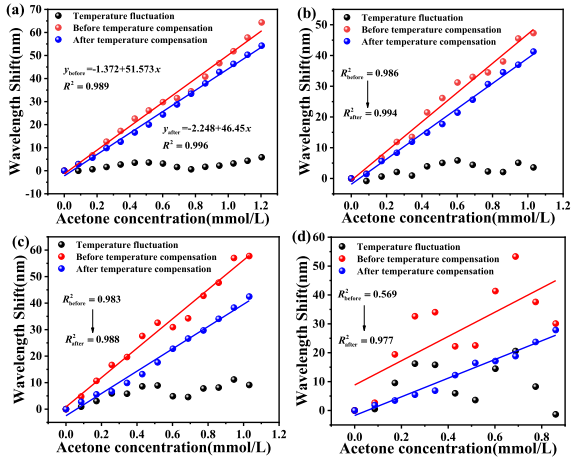

Fig. 5. Temperature compensation of the VOC gas sensor under different temperature fluctuations. Temperature fluctuations caused by (a) airflow, (b) far-distance human breathing, (c) near-distance human breathing, and (d) artificial temperature fluctuation.

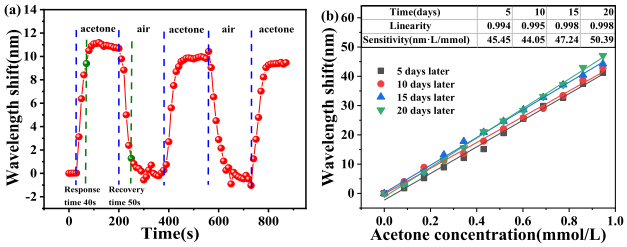

Fig. 6. (a) Dynamic spectral response of the VOC gas sensor in cyclical contact with 0.2 mmol/L acetone. (b) Dependence of the peak wavelength shift on the acetone concentration within 20 days.

start the next cycle. Figure 6(a) presents the peak2 wavelength shifts under three cycles. In all cycles, when the concentration reaches 0.2 mmol/L, the shift is about 10 nm, and when the concentration is 0, the shift returns to 0. After acetone is injected into the gas chamber, the sensor quickly responds. It takes about 40 s to achieve 90% of the equilibrium response [19] and less than 50 s to reach the equilibrium response. After the probe is removed from the gas chamber, it takes about 50 s to restore 90% of the equilibrium response, and 60 s to return the equilibrium response. The residual acetone gas in CLC2 may cause the equilibrium value to slightly drop. These experimental results prove that the proposed VOC gas sensor has exceptional repeatability and fast response time.

Stability is also an important performance of a sensor. Figure 6(b) exhibits the dependence of the peak wavelength shift on the acetone concentration (0–0.946 mmol/L) every five days. In 20 days, the average sensitivity is 46.78 nm·L/mmol, the maximum sensitivity is 50.39 nm·L/mmol, and the maximum sensitivity deviation is only 7.7%. We believe that the sensitivity deviation comes from the minor difference in the amount of acetone solvent injected into the gas chamber each time and the accumulated deviations in the selection of data points.

A simple and label-free temperature-compensated fiber VOC gas sensor based on CLC has been proposed and demonstrated. The linear relationship between the reflection wavelength and acetone concentration has been proved. In addition, the sensor presents an excellent temperature compensation capability to deal with temperature fluctuations. The proposed VOC gas sensor has the advantages of a compact structure, high sensitivity, good repeatability, fast response time, strong stability, and easily recognizable wavelength shift. It can be potentially applied to various VOC gas detection systems, such as the detection of drunk driving and diabetic patients.

Funding. National Natural Science Foundation of China (U1531102, 61975202, 61775212); State Key Laboratory of Applied Optics; Fundamental Research Funds for the Central Universities.

Disclosures. The authors declare no conflicts of interest.

Data Availability. Data underlying the results presented in this paper are not publicly available at this time but may be obtained from the authors upon reasonable request.

REFERENCES

1. D. H. Liang, L. H. Shi, J. X. Liu, S. Ebelt, N. Scovronick, and H. H. Chang, Innovation **1**, 100047 (2020).
2. A. Mirzaei, J. H. Kim, H. W. Kim, and S. S. Kim, J. Mater. Chem. C **6**, 4342 (2018).
3. T. Saidi, O. Zaim, M. Moufid, N. El Bari, R. Ionescu, and B. Bouchikhi, Sens. Actuators B Chem. **257**, 178 (2018).
4. S. Zimmerman, S. Barth, W. K. M. Baether, and J. Ringer, Anal. Chem. **80**, 6671 (2008).
5. H. E. Joe, H. Yun, S. H. Jo, M. B. G. Jun, and B. K. Min, Int. J. Precis. Eng. Manuf.-Green Tech. **5**, 173 (2018).
6. J. Y. Hu, D. Zhou, Y. M. Su, S. Q. Liu, P. X. Miao, Y. C. Shi, W. M. Sun, and Y. J. Liu, Opt. Lett. **45**, 5209 (2020).
7. M. Humar, Liq. Cryst. **43**, 1937 (2016).
8. Y. Wang, L. Zhao, A. Xu, L. Wang, L. Zhang, S. Liu, Y. Liu, and H. Li, Sens. Actuators B Chem. **258**, 1090 (2018).
9. Y. Yang, Y. K. Kim, X. Wang, M. Tsuei, and N. L. Abbott, ACS Appl. Mater. Interfaces **12**, 42099 (2020).
10. J. Y. Hu, D. Y. Fu, C. L. Xia, C. Zhang, L. S. Yao, C. L. Lu, W. M. Sun, and Y. J. Liu, Liq. Cryst. **47**, 508 (2020).
11. Z. R. Xiong, H. Zhang, Y. L. Lu, L. L. Zhang, W. M. Sun, and Y. J. Liu, IEEE Sens. J. **20**, 617 (2019).
12. D. A. Winterbottom, R. Narayanaswamy, and I. M. Raimundo, Jr., Sens. Actuators B Chem. **90**, 52 (2003).
13. L. Sutarlie, H. Qin, and K. L. Yang, Analyst **135**, 1691 (2010).
14. P. V. Shibaev, D. Carrozzi, L. Vigilia, and H. DeWeese, Liq. Cryst. **46**, 1309 (2019).
15. C. K. Chang, H. L. Kuo, K. T. Tang, and S. W. Chiu, Appl. Phys. Lett. **99**, 073504 (2011).
16. J. Y. Tang, J. B. Fang, Y. L. Liang, B. Zhang, Y. H. Luo, X. Y. Liu, Z. B. Li, X. J. Cai, J. Q. Xian, H. Lin, W. G. Zhu, H. Y. Guan, H. H. Lu, J. Zhang, J. H. Yu, and Z. Chen, Sens. Actuators B Chem. **273**, 1816 (2018).
17. Y. H. Yang, D. Zhou, X. J. Liu, S. Q. Liu, P. X. Miao, Y. C. Shi, Y. J. Liu, and W. M. Sun, Opt. Express **28**, 31872 (2020).
18. Q. Zhang, P. Wang, J. Li, and X. Gao, Biosens. Bioelectron. **15**, 249 (2000).
19. D. I. Avsar and E. Bukusoglu, Soft Matter **16**, 8683 (2020).